

Machine Learning-Based COTS Device Process Identification and Total Ionizing Dose Degradation Prediction via Enhanced Electrical Stress Features*

Ji-Cong Yang,^{1,2,3,4} Xiao-Long Li,^{1,2,3} Qi Guo,^{1,2,3,†} Jie Feng,^{1,2,3} Qi-Wen Zheng,^{1,2,3} Lin Wen,^{1,2,3} and Yu-Dong Li^{1,2,3}

¹Key Laboratory of Functional Materials and Devices for Special Environments,
Chinese Academy of Sciences, Urumqi 830011, China

²Xinjiang Key Laboratory of Extreme Environment Electronics, Urumqi 830011, China

³Xinjiang Technical Institute of Physics and Chemistry,
Chinese Academy of Sciences, Urumqi 830011, China

⁴University of Chinese Academy of Sciences, Beijing 101408, China

Commercial Off-The-Shelf (COTS) devices are widely used in aerospace electronic systems, but their process design does not meet the application requirements of the space radiation environment, leading to performance degradation risks caused by Total Ionizing Dose (TID) effects. However, traditional sampling-average radiation hardness (RH) assessment methods are costly and time-consuming, and fail to effectively address lot-to-lot and within-lot fluctuations in the RH consistency of COTS devices. This paper proposes a machine learning model based on physical feature enhancement. A high-quality dataset is constructed via irradiation experiments on devices from multiple manufacturers and lots. By introducing electrical parameter responses under multiple electrical stress conditions as enhanced feature parameters, the model realizes non-destructive identification of device manufacturing processes and prediction of total-dose radiation degradation. Results show that the model achieves identification accuracy of approximately 0.965 for device manufacturers and 0.842 for lots; at four specific dose points, the coefficient of determination (R^2) for radiation degradation prediction is above 0.838, outperforming the sampling-average prediction method. Incorporating electrical parameter responses under multiple electrical stress conditions improves the model's performance in manufacturing process identification and TID radiation degradation prediction. This study reveals that differences in the pre-irradiation initial electrical parameters of devices have an implicit correlation with their radiation hardness characteristics. Compared with a single test condition, the responses of device parameters to multiple electrical stresses contain richer RH feature information. In addition, the model is verified to have certain generalization ability on new lot samples not included in the training set. This method provides a new approach for the efficient screening and assessment of the radiation hardness of COTS devices.

Keywords: Commercial Off-The-Shelf, Total Ionizing Dose, Machine Learning, Radiation Hardness, Feature Enhancement

This work was supported by the NSAF Joint Fund (Grant No. E5111102), the Tianshan Innovation Team (Grant No. 2023TSYCTD0010), the Strategic Priority Research Program of the Chinese Academy of Sciences (Grant No. XDB1200102), the Key Research and Development Program of Xinjiang (Grant No. 2023B01008), the National Natural Science Foundation of China (Grant No. U2530216), and the Tianshan Talents Program (Grant No. 2024TSYCCX0085).

Corresponding author, Qi Guo, No.40-1, South Beijing Road, Urumqi, guoqi@ms.xjb.ac.cn.

I. Introduction

COTS devices are increasingly widely used in aerospace electronic systems. Such devices offer advantages including high performance, low cost, short development cycles, mass production capability, and ease of integrating new materials and technologies [1-3]. However, when COTS devices are deployed in the space radiation environment, they are affected by TID effects, leading to electrical performance degradation and failure [4-7]. Moreover, their design and manufacturing are oriented toward general-

purpose applications, without considering the special requirements of the space radiation environment, and they lack dedicated design and reliability assurance measures [8, 9]. Therefore, developing non-destructive screening and effective assessment of the RH of COTS devices has become a core prerequisite for ensuring the on-orbit reliability of aerospace electronic systems.

In the assessment of RH of lot devices, traditional sampling-averaged methods typically assume high RH consistency among samples and, on this basis, perform sampling inspection to obtain unbiased estimates of population parameters through random samples. However, when such methods are applied to evaluate the suitability of COTS devices for the special radiation environment, two critical issues arise. First, the lot-to-lot consistency of RH for traditional space-grade devices is ensured by strict manufacturing process control, whereas the design, process, and quality control systems of COTS devices do not cover RH requirements. Moreover, information on the manufacturing process is often difficult to obtain, making it challenging to effectively guarantee the lot-to-lot consistency of RH for COTS devices. Second, the sampling-averaged assessment method involves difficult experiments, high cost, and long cycle times. If a mapping relationship between the pre-irradiation electrical parameters of a device and its RH performance can be established as a fingerprint of its RH, enabling the prediction of TID degradation using only initial values, then non-destructive screening can be achieved, reducing cost and cycle time.

Machine learning techniques have demonstrated broad applicability across many scientific fields, including materials design [10, 11], drug discovery [12], genomic analysis [13], and nuclear physics research [14-16]. Their core advantage lies in effectively integrating experimental data with theoretical models, uncovering complex nonlinear relationships that are difficult to capture with traditional methods, and revealing underlying mechanisms [17]. Neural networks, with their powerful nonlinear mapping capabilities, have shown good potential for function fitting and regression prediction tasks [18, 19].

In recent years, machine learning methods have been applied to the field of radiation effects. Fernando Morilla et al. proposed an Advanced Predictor of

Electrical Parameters (APEP) method based on machine learning. This method consists of two stages: "degradation pattern recognition in a database" and "degradation prediction for unirradiated new samples." Relying on historical data from the PRECEDER radiation test database, it predicts the degradation of electrical parameters of devices under TID radiation. Using bipolar junction transistors (BJTs) as validation objects, the method achieves good prediction results under both biased and unbiased irradiation conditions through both data-driven and model-driven approaches. It reduces destructive testing, simplifies experimental setups, and lowers costs, and the methodology has the potential to be extended to other microelectronic components [20, 21]. Additionally, the team of Wang Baichuan constructed and trained an artificial neural network (ANN)-based model using TID effect data of BJTs from different experiments. The results show that the model significantly outperforms traditional multiple linear regression methods in capturing nonlinear correlations and predicting data. The trained ANN model revealed that the TID radiation resistance of BJTs increases with the initial value of the base current. Through mechanistic analysis, the researchers suggested that the difference in emitter perimeter-to-area ratio may be one reason for this phenomenon, and they verified this conclusion through irradiation experiments [22].

The above studies demonstrate the feasibility of machine learning for TID degradation prediction. However, due to the strict quality control of COTS devices, conventional electrical parameters exhibit high consistency, and existing methods all use electrical parameters obtained by standard test methods as training data, making it difficult to fully capture fingerprint information of RH.

This paper proposes a TID effect degradation prediction model for COTS BJTs based on machine learning methods. By extracting the electrical parameter responses of unirradiated devices under multiple sets of electrical stresses, a feature engineering approach rich in physical information is constructed. Combined with an interpretable neural network architecture, the model achieves identification of process information and prediction of TID degradation for COTS BJTs using only the electrical parameter data of unirradiated samples. The method proposed in this paper provides a new

technical approach for radiation hardness assurance (RHA) research of COTS devices.

II. Materials and Methods

2.1 Experimental samples

To obtain a high-quality dataset, consistency of experimental conditions must be ensured. BJTs feature a relatively simple structure, their TID effect mechanisms have been extensively studied, and abundant experimental data have been accumulated. Therefore, using BJTs as the initial carrier for TID degradation prediction research on COTS devices offers both theoretical and experimental advantages [23-26]. Based on this, this study conducts TID irradiation experiments on COTS BJTs from multiple manufacturers and lots, aiming to provide reliable data support for the subsequent training, validation, and testing of the neural network model.

To ensure the representativeness and statistical validity of the samples, a total of 570 samples were selected in this study. The manufacturers, part number, lots, and quantity distributions of these samples are detailed in Table 1.

2.2 Experimental test methods

Irradiation experiments were conducted at the Co-60 γ -ray facility of the Xinjiang Technical Institute of Physics and Chemistry, Chinese Academy of Sciences (XTIPC, CAS). For each experiment, 70 samples were selected and irradiated simultaneously at room temperature. Previous studies have shown that BJTs exhibit

the most severe degradation under zero bias conditions in a TID radiation environment [27]. Therefore, in this study, the devices were placed on an irradiation board with all pins shorted and grounded for irradiation tests. The dose rate was 50 rad(Si)/s, and the total dose was 100 krad(Si). When the accumulated dose of the samples reached 25 krad, 50 krad, 75 krad, and 100 krad, the samples were immediately subjected to post-irradiation testing.

Post-irradiation testing was performed using the BC3193 semiconductor discrete device test system at XTIPC. To obtain more comprehensive RH characteristic information of the devices, additional tests under multiple sets of electrical stress conditions were added on the basis of the tests conducted under the conditions specified in the device datasheets. By applying different electrical bias conditions, the characteristic differences in radiation-sensitive regions such as the oxide layer of the devices were introduced into the responses of electrical parameters, thereby enhancing the physical features related to RH. The specific test contents are shown in Table 2. In the following text, tests performed under the conditions specified in the device datasheets are defined as conventional parameter tests, while the remaining tests under other electrical stresses are classified as enhanced parameter tests. Pre-irradiation (0 krad) measurements included both conventional and enhanced parameter tests; at each irradiation dose point, only conventional parameters were tested. For each device, hFE tests under four sets of electrical stress conditions were conducted before irradiation, including three sets of conventional test conditions from different manufacturers and one set under a high injection current condition. Under the high injection current bias, the BJT enters the Kirk effect operating region [28, 29].

2.3 Dataset

Through the irradiation experiments and device tests described in Section 2.2, the experimental test data of 570 BJTs were constructed into a dataset in this study. Fig. 1, taking hFE as an example,

Table 1 Device Selection

Manufacturer	Part Number	Lot	Sample Quantity (device)
MUL	2N2222A	S7	70
MUL	2N2222A	JB	70
MUL	2N2222A	H7	70
JINAN	3DK2222	J24.3	70
JINAN	3DK2222	J24.4	70
JINAN	3DK2222	J25.1	50
SHI	F2N2222	2208	50
SHI	F2N2222	2312	50
SHI	F2N2222	2405	70

Table 2 Parameters and Test Information

Type	Parameter	Test Condition
Regular parameter	$VCEsat_{reg}$	$IB=IB_{reg},$ $IC=IC_{reg}$
Regular parameter	$VBEsat_{reg}$	$IB=IB_{reg},$ $IC=IC_{reg}$
Regular parameter	$Vceo_{reg}$	$IB=0mA,$ $IC=IC_{reg}$
Regular parameter	$Icbo_{reg}$	$VCB=VCB_{reg},$ $IE=0mA$
Regular parameter	$Iebo_{reg}$	$VEB=VEB_{reg},$ $IC=0mA$
Regular parameter	hFE_{reg}	$VCE=VCE_{reg},$ $IC=IC_{reg}$
Enhanced parameter	hFE_{Other1}	$VCE=VCE_{Other1},$ $IC=IC_{Other1}$
Enhanced parameter	hFE_{Other2}	$VCE=VCE_{Other2},$ $IC=IC_{Other2}$
Enhanced parameter	hFE_{Kirk}	$VCE=VCE_{reg},$ $IC=0.9IC_{max}$
Enhanced parameter	$VCEsat_{highIC}$	$IB=IB_{reg},$ $IC=0.9IC_{max}$
Enhanced parameter	$VBEsat_{highIC}$	$IB=IB_{reg},$ $IC=0.9IC_{max}$

[Other number] denotes the regular test condition of a different manufacturer.

illustrates the distribution of electrical parameters of unirradiated devices in the dataset. The results show that differences in manufacturer and lot, i.e., device process variations, directly lead to fluctuations in the numerical distribution of device electrical parameters, and the numerical distribution of electrical parameters for individual lots is relatively dispersed. Furthermore, variations in electrical stress test conditions can effectively reveal differences in the internal process structures of the devices. Such process differences are ultimately reflected in the distribution of hFE parameters under unirradiated conditions [30-32]. For example, in Fig. 1(a), under regular electrical stress, the hFE values of the H7 lot from the MUL manufacturer are generally higher than those of the S7 and JB lots. Under the high injection current condition, however, the hFE values of the H7 lot lie between those of the S7 and JB lots.

Therefore, in this study, the numerical differences in hFE , VCE, and VBE parameters measured under regular and high injection current conditions were quantified as new features, serving as additional bases for analyzing the internal process characteristics of the devices. The calculation formulas for the new features are given as Eq.##(1), (2), (3).

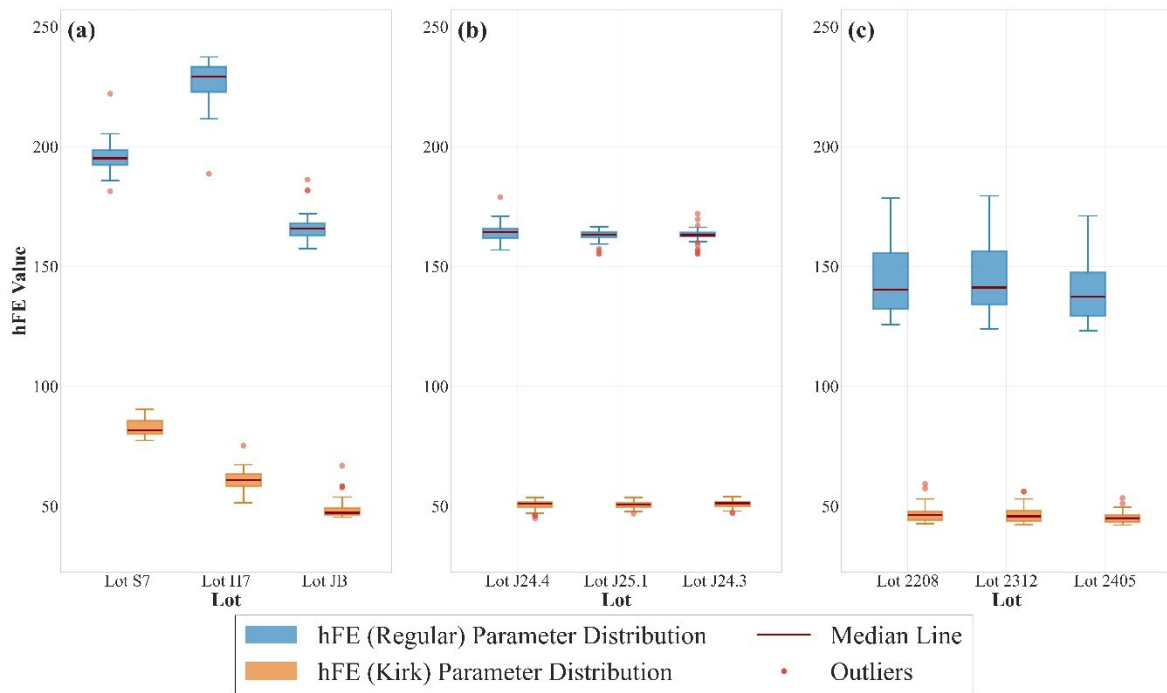


Fig. 1 hFE value distribution under different electrical stresses for different manufacturers and lots (0 krad). (a) MUL manufacturer, (b) JINAN manufacturer, (c) SHI manufacturer.

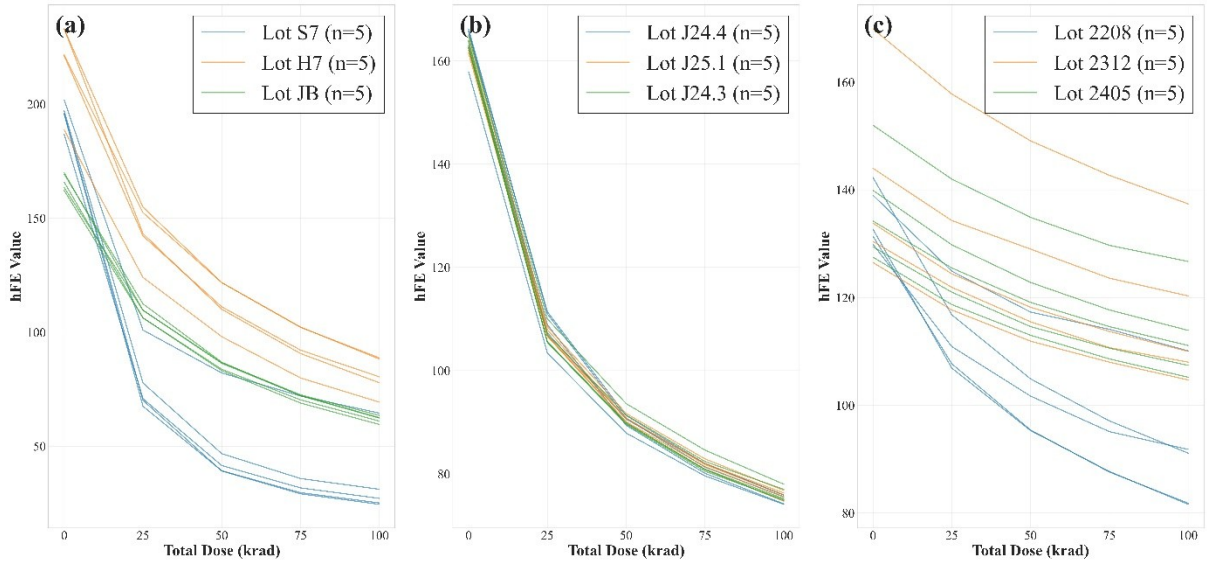


Fig. 2 Example TID radiation degradation curves of devices from different manufacturers and lots (5 devices per lot, $n=5$). (a) MUL manufacturer, (b) JINAN manufacturer, (c) SHI manufacturer.

$$hFE_{diff} = \frac{hFE_{reg} - hFE_{Kirk}}{hFE_{reg}} \quad (1)$$

$$VCE_{diff} = \frac{VCE_{sat_{reg}} - VCE_{sat_{highIC}}}{VCE_{sat_{reg}}} \quad (2)$$

$$VBE_{diff} = \frac{VBE_{sat_{reg}} - VBE_{sat_{highIC}}}{VBE_{sat_{reg}}} \quad (3)$$

In this study, five device samples from each lot were selected for comparative analysis of radiation degradation data. The results shown in Fig. 2 indicate that differences introduced by device structure and process also lead to fluctuations in device radiation sensitivity. For batches with similar distributions of initial electrical parameter values, such as Fig. 2 J24.3, J24.4, and J25.1, the differences in degradation rates between batches are relatively small; conversely, for batches with dissimilar distributions, such as Fig. 2(a) S7, JB, and H7, the differences are larger. Overall, the difference in degradation rate between different manufacturers is generally larger than that between different batches from the same manufacturer. However, it should be noted that the degree of similarity in device radiation degradation rates cannot be directly judged solely based on the distribution of initial electrical parameter values. As shown in Fig. 2(c), the initial electrical parameter values of some devices in batch 2208 fall within the

distribution range of batches 2312 and 2405, yet their degradation rates differ significantly from those of the latter two batches. Therefore, identifying device process variations arising from differences in manufacturer and batch is an important prerequisite for assessing device RH.

The above analysis indicates that the initial values of device electrical parameters can not only reflect manufacturing process differences among different manufacturers and lots, but also contain precursor information implicitly correlated with device radiation hardness. In most cases, lot-to-lot differences also lead to distinct radiation degradation patterns in devices. Although traditional machine learning clustering algorithms can preliminarily identify degradation patterns in a dataset, their results are susceptible to data noise from individual lots, leading to errors in degradation pattern classification for new samples and consequently reducing the accuracy of device radiation degradation prediction.

2.4 Model architecture

In this study, the dataset is divided into training, validation, and test sets at a ratio of 8:1:1 in terms of the number of devices. Based on the feature engineering shown in Table 3, a BJT RH assessment model is constructed. Specifically, traditional machine learning algorithms are employed for manufacturer and lot identification,

Table 3 Feature Engineering

DC Parameter Features [#]	Multi- Condition <i>hFE</i> Features ^{##}	High- Injection Current Electrical Stress Features ^{##}	Relative Difference Features ^{##}
<i>hFE_{reg}</i>		<i>hFE_{Kirk}</i>	<i>hFE_{diff}</i>
<i>VCEsat_{reg}</i>	<i>hFE_{Other1}</i>		
<i>VBEsat_{reg}</i>		<i>VCEsat_{highIC}</i>	<i>VCE_{diff}</i>
<i>Vceo_{reg}</i>			
<i>Icbo_{reg}</i>	<i>hFE_{Other2}</i>	<i>VBEsat_{highIC}</i>	<i>VBE_{diff}</i>
<i>Iebo_{reg}</i>			

[#] denotes regular features, [##] denotes enhanced features.

and an ANN is used for radiation degradation prediction. This scheme aims to fully exploit the underlying patterns in the data and enhance the model's learning capability for the radiation degradation characteristics of devices from different manufacturers and lots.

2.4.1 Manufacturer and lot identification

In the manufacturer identification model, the system adopts a pattern matching method based on statistical data distribution. During the training phase, the system constructs a baseline distribution model for each electrical parameter for every manufacturer. The reasonable range of each parameter is statistically determined using the quartile method, with the lower and upper bounds defined as $[Q_1 - 1.5 \times IQR]$ and $[Q_3 + 1.5 \times IQR]$ [33], respectively. In the inference phase, each parameter value of a new sample is compared with the parameter ranges of each manufacturer, and a probability update mechanism for manufacturer identification is employed: if the parameter value falls within the range of a given manufacturer, its probability weight is increased; otherwise, it is decreased. The manufacturer with the highest probability is finally selected as the prediction result, and its normalized probability serves as the identification confidence. This method is intuitive and robust, and is particularly suitable for identification scenarios involving manufacturers with small sample sizes.

To effectively identify subtle electrical differences among different lots from the same

manufacturer, this study employs Random Forest as the core algorithm of the lot identification model. By constructing multiple decision trees and aggregating their voting results, the algorithm can effectively handle nonlinear interactions among high-dimensional features without requiring normalization of the feature value ranges, and it possesses anti-overfitting capability. The algorithm input includes all features mentioned in Table 3. During training, a separate classifier is trained for each manufacturer to fully capture lot-specific characteristics under different manufacturing processes. Each Random Forest classifier is configured with 100 decision trees, a maximum depth of 10, a minimum number of samples required to split an internal node of 2, and a minimum number of samples required at a leaf node of 1. Class imbalance is addressed by balancing class weights.

2.4.2 TID radiation degradation prediction

For an NPN BJT, total ionizing dose introduces interface states (*N_{it}*) and oxide trapped charge (*N_{ot}*) at the Si/SiO₂ interface, significantly enhancing the surface recombination in the base region. This causes a marked increase in the base current *I_B* in the low *V_{BE}* region. Meanwhile, the collector current *I_C*, dominated by bulk minority carrier diffusion, is insensitive to interface defects and remains essentially unchanged. As a key performance metric, the common-emitter current gain ($hFE = I_C / I_B$) therefore degrades significantly at low *V_{BE}*, and the peak gain shifts toward higher forward bias with increasing accumulated dose. In bipolar linear integrated circuits, current gain degradation is the most typical failure mechanism under total ionizing dose effects. Based on the above physical principles, this study selects the *hFE* retention rates at dose points of 25, 50, 75, and 100 krad as the output parameters of the neural network model for predicting radiation degradation. The *hFE* retention rate normalizes the initial dispersion of devices and intuitively characterizes the remaining performance of devices after irradiation. Its calculation formula is given as Eq.(4). *hFE_{now}* is the *hFE* value at a given dose point, and *hFE_{reg}* is the pre-irradiation *hFE* value.

$$hFE_{retention} = \frac{hFE_{now}}{hFE_{reg}} \quad (4)$$

The neural network architecture employed in this study is shown in Fig. 3. The neural network adopts a hierarchical fusion architecture consisting of four core modules: a relative difference feature processor (3→64 nodes) processing the relative difference features, an other feature processor (12→64 nodes) processing the features other than the relative difference features, a feature fusion layer (128→128→64 nodes) integrating the feature information, and a prediction head (64→32→4 nodes) outputting the degradation rates at four dose points. After each linear layer, a Sigmoid Linear

Unit (SiLU) activation function, Layer Normalization, and Dropout regularization are applied [34-36]. Finally, the output range is constrained to [0.1, 0.95] by a Sigmoid function to ensure that the predicted values conform to the basic physical definitions.

During model training, the validation set serves to monitor optimization. To balance training speed and convergence stability, the training employs mean squared error (MSE) as the loss function,

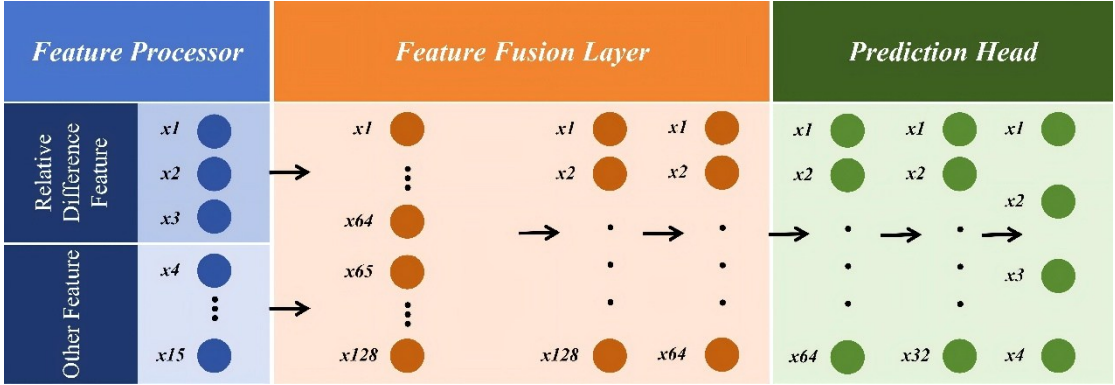


Fig. 3 Schematic diagram of the neural network architecture for TID radiation degradation prediction.

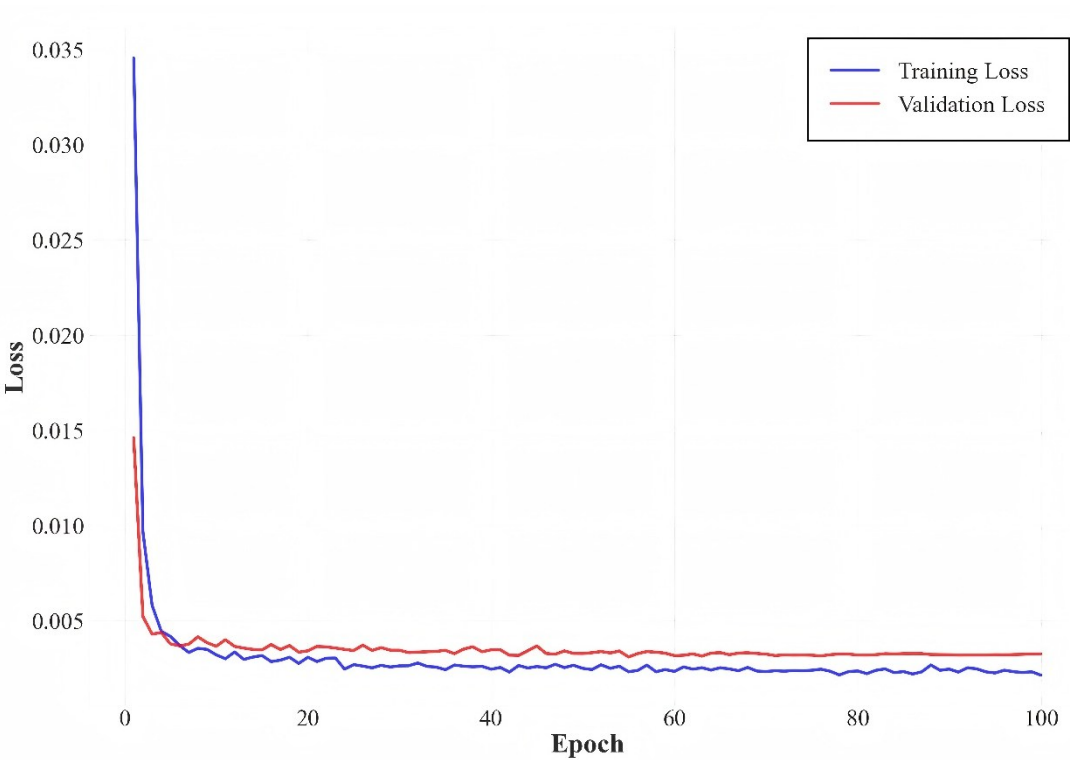


Fig. 4 Training and validation loss curves. The model converges steadily after approximately 40 epochs, with no significant overfitting observed.

Table 4 Test set sample information

MUL			JINAN			SHI		
S7	JB	H7	J24.3	J24.4	J25.1	2208	2312	2405
7	7	7	7	7	5	5	5	7

Eq.(5), and the optimizer uses the Adam algorithm with adaptive learning rate, combined with a learning rate decay strategy (ReduceLROnPlateau) [37, 38]. When the validation loss shows no improvement for 10 consecutive epochs, the learning rate is halved. This dynamic adjustment mechanism effectively balances training speed and convergence stability. The convergence process of the model is shown in Fig. 4. The model converges stably after 100 training epochs, with a minimum validation loss of approximately 0.002, and no overfitting is observed.

$$MSE = \frac{1}{n} \sum_{i=1}^n (y_i - \hat{y}_i)^2 \quad (5)$$

n is the number of samples, y_i is the true value of the i -th sample, and \hat{y}_i is the predicted value of the i -th sample.

III. Results and Discussion

Using an independent test set, the effectiveness of the proposed method in process category identification and radiation degradation prediction tasks is verified, and its physical mechanism and generalization ability are analyzed. The information of the test set samples is shown in Table 4.

3.1 Process identification performance

After the training of the BJT RH assessment model is completed, the manufacturer identification model is invoked to verify the manufacturer and lot identification on 57 device samples in the test set. The manufacturer identification confusion matrix in Fig. 5 shows that the model achieves good performance in the manufacturer identification task, with an overall identification accuracy of 0.965 and an average confidence of 0.948. Combined with Fig. 1, BJTs from different manufacturers exhibit inherent differences in core device structures such as doping profiles and Si/SiO₂ interface processes, which directly lead to clear process-related

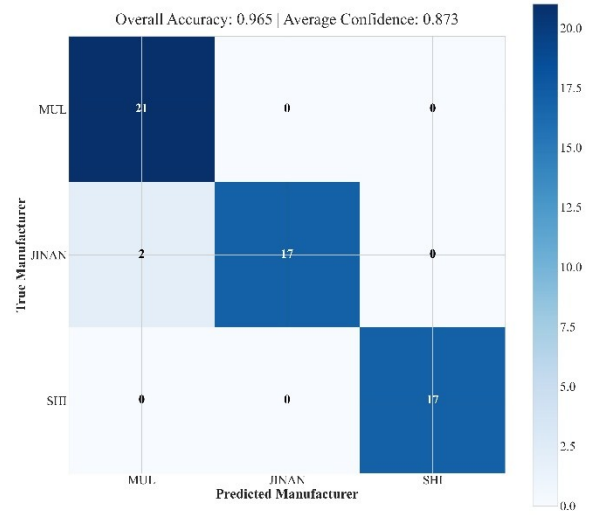


Fig. 5 Manufacturer identification confusion matrix. Diagonal elements represent the number of correctly identified samples, while off-diagonal elements represent the number of misclassified samples. Manufacturer identification accuracy is the proportion of correctly predicted samples in the test set, and confidence is the average of the maximum probability values output by the Random Forest model for each sample prediction in the test set.

differences in the initial electrical parameter characteristics of the devices, resulting in high feature discriminability. Therefore, high-precision manufacturer identification can be achieved.

The lot identification confusion matrix shown in Fig. 6 indicates that the constructed Random Forest model also achieves reliable identification performance in the lot identification task, with an overall identification accuracy of 0.842 and an average confidence of 0.722. Combined with Fig. 1, compared with the significant parameter discriminability resulting from differences in device structure and core processes among different manufacturers, devices from different lots of the same manufacturer exhibit only minor electrical differences caused by process line switching. The initial distributions of device electrical parameters have wide overlapping regions, and the feature discriminability is much weaker than that in the manufacturer identification scenario. Nevertheless,

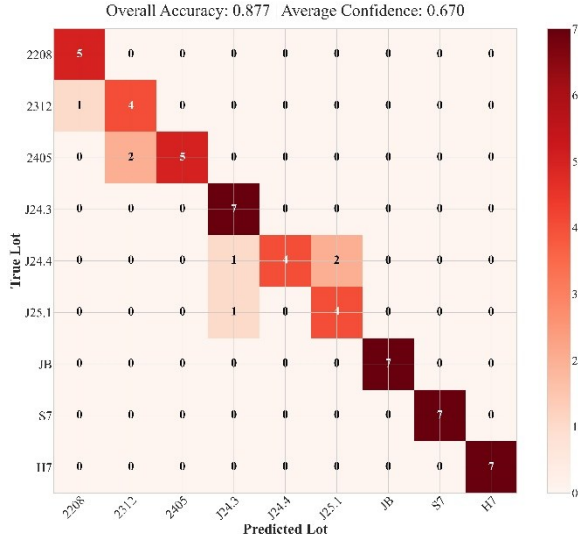


Fig. 6 Lot identification confusion matrix. Diagonal elements represent the number of correctly identified samples for each lot, while off-diagonal elements represent the number of misclassified samples. The lot identification accuracy is obtained by comparing the predicted labels of the test samples with the true labels one by one and calculating the proportion of correct predictions. The confidence is derived as the arithmetic mean, over the test set, of the maximum class probability output by the Random Forest for each sample.

the adopted Random Forest algorithm can effectively mine weak correlation information in high-dimensional features, thereby achieving stable and reliable lot identification even under conditions of high parameter overlap among lots.

The above results indicate that the COTS BJT manufacturing process identification method based on device electrical parameter characteristics under multiple sets of electrical stresses exhibits high reliability and stability. The prior information of manufacturing processes obtained by this method can provide key process constraints for the subsequent device radiation degradation prediction model.

3.2 TID radiation degradation prediction performance

Using the trained BJT RH assessment model, TID degradation prediction was further validated on test set samples with known manufacturing process information. The results are shown in Fig. 7. The model predictions are in good agreement

with the experimental measurements, and the true values at all four dose points lie within the 90% confidence intervals of the predicted values.

To quantitatively evaluate the radiation degradation prediction performance of the model on the test set, this study employs three metrics: coefficient of determination (R^2), mean absolute error (MAE), and root mean square error (RMSE), with their calculation formulas given as Eq. (6), (7), (8). R^2 is used to measure the model's ability to explain the fluctuations in device radiation degradation parameters and the improvement over sampling-average prediction. MAE intuitively reflects the average magnitude of prediction errors, while RMSE is more sensitive to large errors.

$$R^2 = 1 - \frac{\sum_{i=1}^n (y_i - \hat{y}_i)^2}{\sum_{i=1}^n (y_i - \bar{y})^2} \quad (6)$$

$$MAE = \frac{1}{n} \sum_{i=1}^n |y_i - \hat{y}_i| \quad (7)$$

$$RMSE = \sqrt{\frac{1}{n} \sum_{i=1}^n (y_i - \hat{y}_i)^2} \quad (8)$$

n is the number of samples, y_i is the true value of the i -th sample, and \hat{y}_i is the predicted value of the i -th sample. \bar{y} is the average of the true values.

The evaluation results of TID degradation prediction performance shown in Fig. 8 indicate that the neural network model constructed in this study achieves high consistency between the predicted and measured hFE retention rates at dose points of 25, 50, 75, and 100 krad. The R^2 values at each dose point are approximately 0.871, 0.867, 0.85, and 0.838, respectively, all outperforming the sampling-average method. The maximum MAE and RMSE are 0.068 and 0.082, respectively. These results demonstrate that the initial values of device electrical parameters contain effective information reflecting their RH.

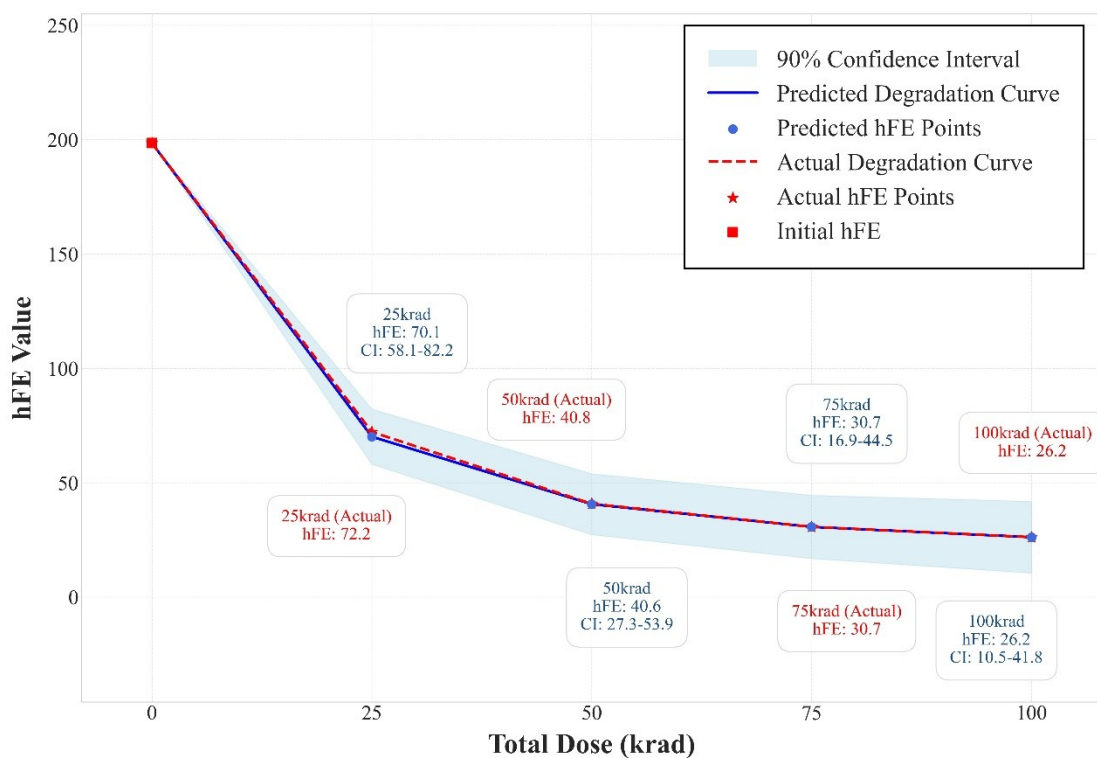


Fig. 7 Comparing TID radiation degradation curves of BJTs. Predicted information in blue, true information in red. "ci" denotes the upper and lower bounds of the 90% confidence interval based on the predicted values.

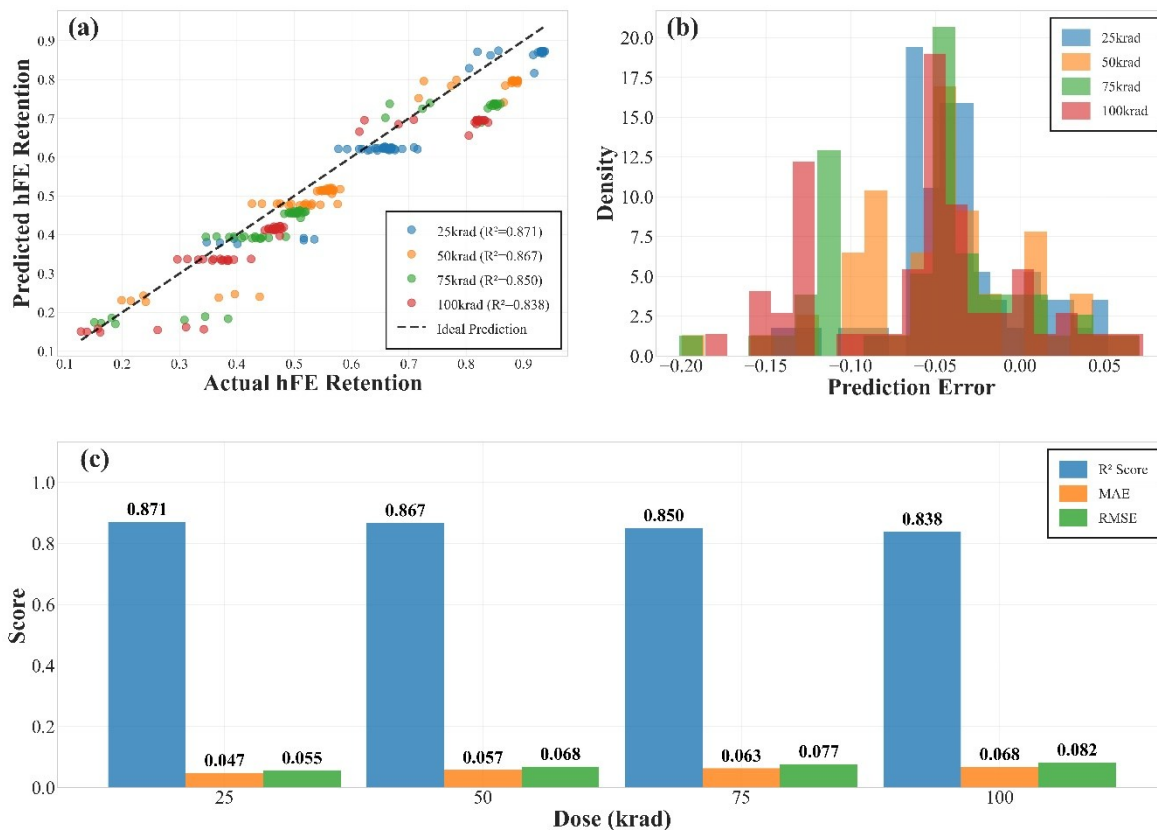


Fig. 8 Evaluation of TID radiation degradation prediction. (a) Scatter plot of predicted vs. actual values: the closer the points are to the diagonal, the more accurate the prediction; (b) Histogram of prediction error distribution: errors concentrated around zero indicate unbiasedness; (c) Bar chart of R^2 , MAE, and RMSE at each dose point, comprehensively evaluating model performance.

3.3 Feature enhancement effectiveness

By toggling the enabling and disabling of the high-injection current electrical stress, relative difference, and multi-condition *hFE* features via Boolean switches, a parallel model performance evaluation scheme with two feature configurations was constructed. Under the condition that the training set, validation set, and model architecture were kept completely identical, the core metrics of manufacturer and lot identification accuracy, as well as R^2 and MAE for radiation degradation prediction, were compared on the same test set. The slight fluctuations in the TID degradation prediction metrics in different comparison plots in this section are normal results of multiple random trainings of the model.

Fig. 9 shows that the high-injection current electrical stress and relative difference features can effectively improve model performance in multi-task scenarios. In the manufacturer and lot identification tasks, the model with these features achieved identification accuracies of 0.965 and 0.836, and average confidences of 0.948 and 0.722, respectively. After removing these features, both identification accuracy and confidence decreased significantly. This result indicates that such features can effectively amplify the electrical manifestation

differences of device manufacturing process variations. By leveraging the physical characteristic that the carrier transport path approaches the oxide-semiconductor interface under the Kirk effect, these features selectively amplify the electrical responses of process-sensitive microstructural features such as interface defects and oxide charges, thereby enhancing the model's ability to capture microstructural differences among different process lots.

In the radiation degradation prediction task, the model with these features achieved an R^2 of 0.849 and an MAE as low as 0.059; after removal, R^2 dropped to 0.598 and MAE increased to 0.088. This result demonstrates that such features play an important role in enabling the model to capture device degradation patterns. By applying such electrical stresses, the internal electric field and carrier distribution of the device can be modulated, effectively amplifying the electrical differences of radiation-sensitive precursors such as radiation-induced interface defects and oxide charges. Using their electrical responses together with relative differences as model inputs significantly enhances the ability of the feature matrix to characterize the physical mechanisms of device radiation degradation and the information related to radiation hardness.

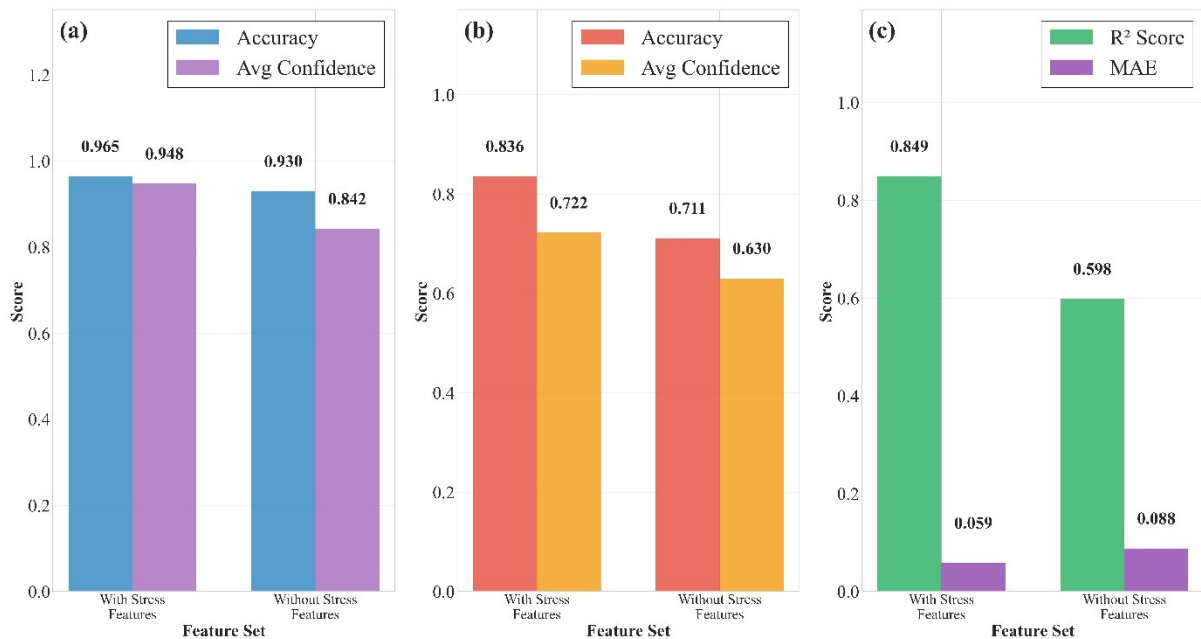


Fig. 9 Influence of High-Injection Current Electrical Stress Features and Relative Difference Features on Manufacturer Identification, Lot Identification, and TID Radiation Degradation Prediction Performance

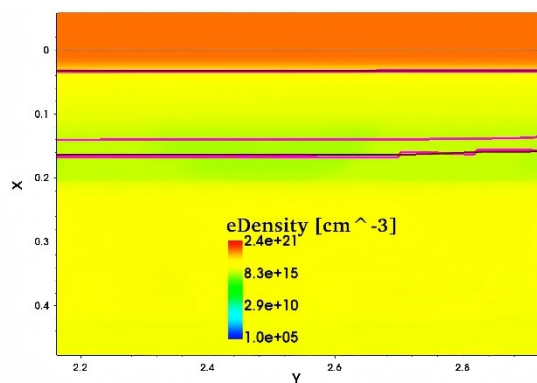


Fig. 10 Under low current density conditions, the depletion region boundary (pink line) inside a BJT is distributed mainly near the collector-base junction.

In an NPN BJT, the high-injection condition corresponding to a high collector current density triggers the Kirk effect, a process that can be directly characterized by the evolution of the electron density distribution inside the device and the boundary of the collector-base depletion region. Under low-injection conditions (Fig. 10), the collector-base depletion region is dominated by ionized impurities in the lightly doped N-type region of the collector. The electron density distribution inside the device is generally uniform, and the boundary of the collector-base depletion region is stable and planar, indicating that the space charge distribution is not significantly perturbed by the injected carriers.

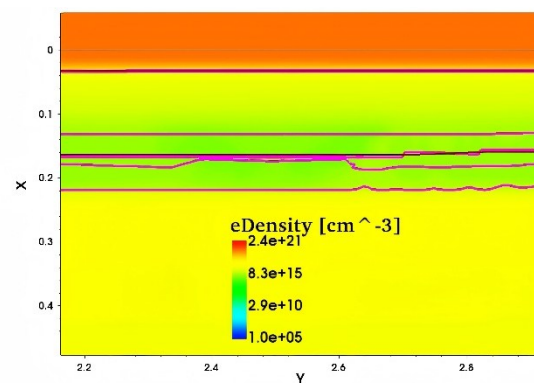


Fig. 11 Under high current density conditions when the Kirk effect occurs, the depletion region boundary (pink line) significantly expands toward the interior of the collector region, and the effective base width increases.

When the bias is increased to a high current density (Fig. 11), the electron concentration injected into the collector-base depletion region exceeds the N-type doping concentration in the collector. The space charge distribution becomes dominated by the injected carriers, forcing the collector-base depletion region to expand significantly toward the collector side. This is manifested as a broadening of the low-electron-density region and a shift of the depletion region boundary toward the collector, thereby inducing base widening. This effect ultimately leads to electrical degradation behaviors such as a decrease in the current gain of the device.

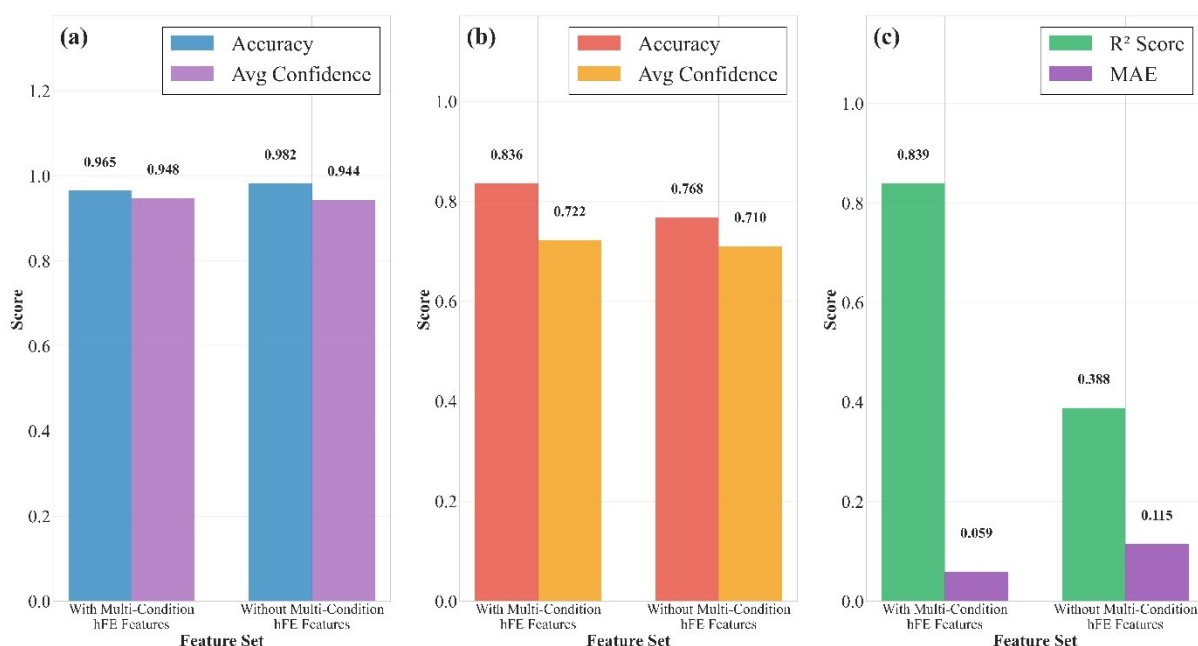


Fig. 12 Influence of Multi-Condition *hFE* Features on Manufacturer Identification, Lot Identification, and TID Radiation Degradation Prediction Performance.

Multi-condition *hFE* features also effectively improve model performance in multi-task scenarios, as shown in Fig. 12. When the multi-condition *hFE* features are disabled, the model performance in the manufacturer identification task shows no significant fluctuation. In the lot identification task, however, the model accuracy drops from 0.836 to 0.768, and the average confidence decreases from 0.722 to 0.71. In the radiation degradation prediction task, the model R^2 decreases from 0.839 to 0.388, and the MAE increases from 0.059 to 0.115. The above fluctuations indicate that the multi-condition *hFE* features can capture process-induced differences in core parameters such as emitter injection efficiency and base minority carrier lifetime of the BJT under different biases, enriching the physical information of the feature matrix, thereby enhancing the model's ability to resolve process variations and improving the prediction accuracy of radiation degradation trends. Combined with the observed improvement in TID degradation prediction brought by the high-

injection current electrical stress features, it can be seen that appropriately modulating the electrical stress amplitude can enhance the capability of feature engineering to characterize the precursor information related to device radiation hardness.

3.4 Lot generalization performance

To verify the generalization ability of the proposed model for TID degradation prediction on unknown new lots, this section reconfigures the dataset splitting strategy: specifically, samples from lot J24.4 are completely excluded from the training and validation sets and are used solely as an independent test set to evaluate model performance. The evaluation results shown in Fig. 13 indicate that the model still possesses a certain generalization potential for unknown new lots from the same manufacturer. For lot J24.4, the minimum R^2 is 0.065, demonstrating the model's basic ability to capture the degradation trend of the new lot.

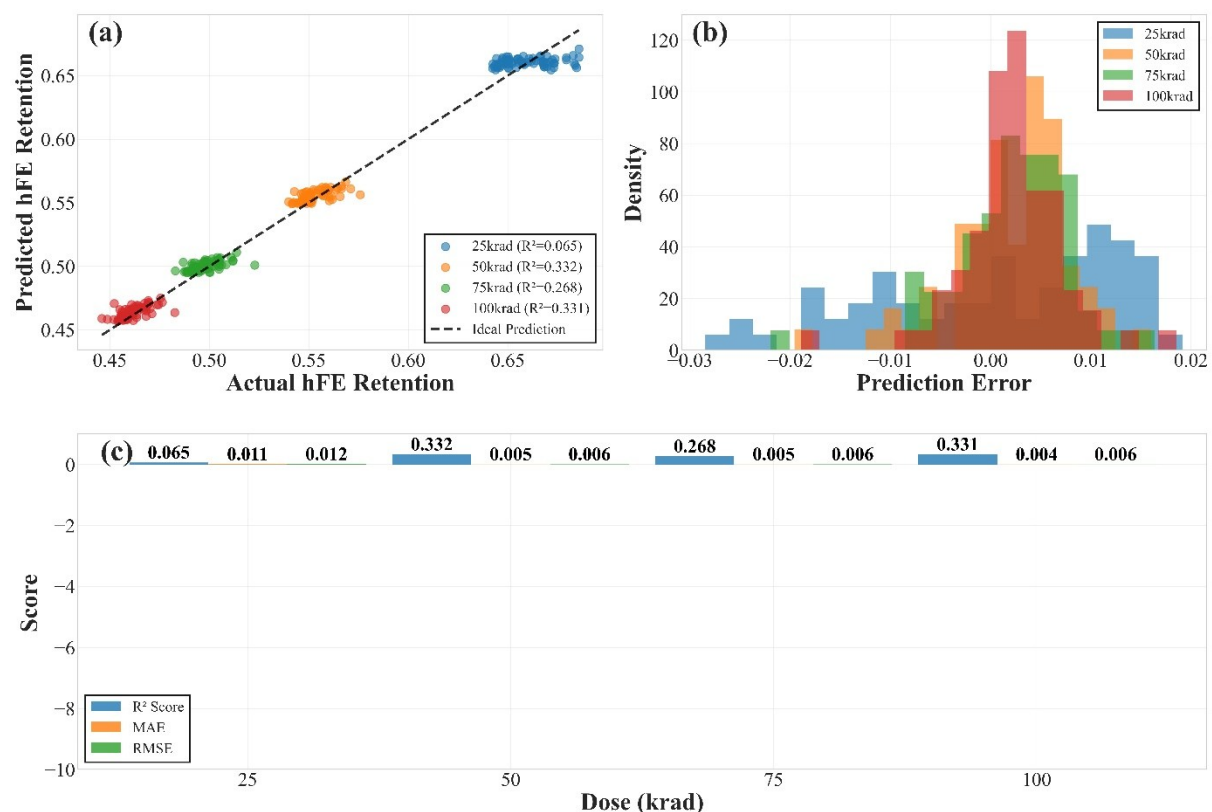


Fig. 13 TID radiation degradation prediction performance of the BJT RH assessment model on unknown new lots (a) Scatter plot of predicted vs. actual values: the closer the points are to the diagonal, the more accurate the prediction; (b) Histogram of prediction error distribution: errors concentrated around zero indicate unbiasedness; (c) Bar chart of R^2 , MAE, and RMSE at each dose point, comprehensively evaluating model performance.

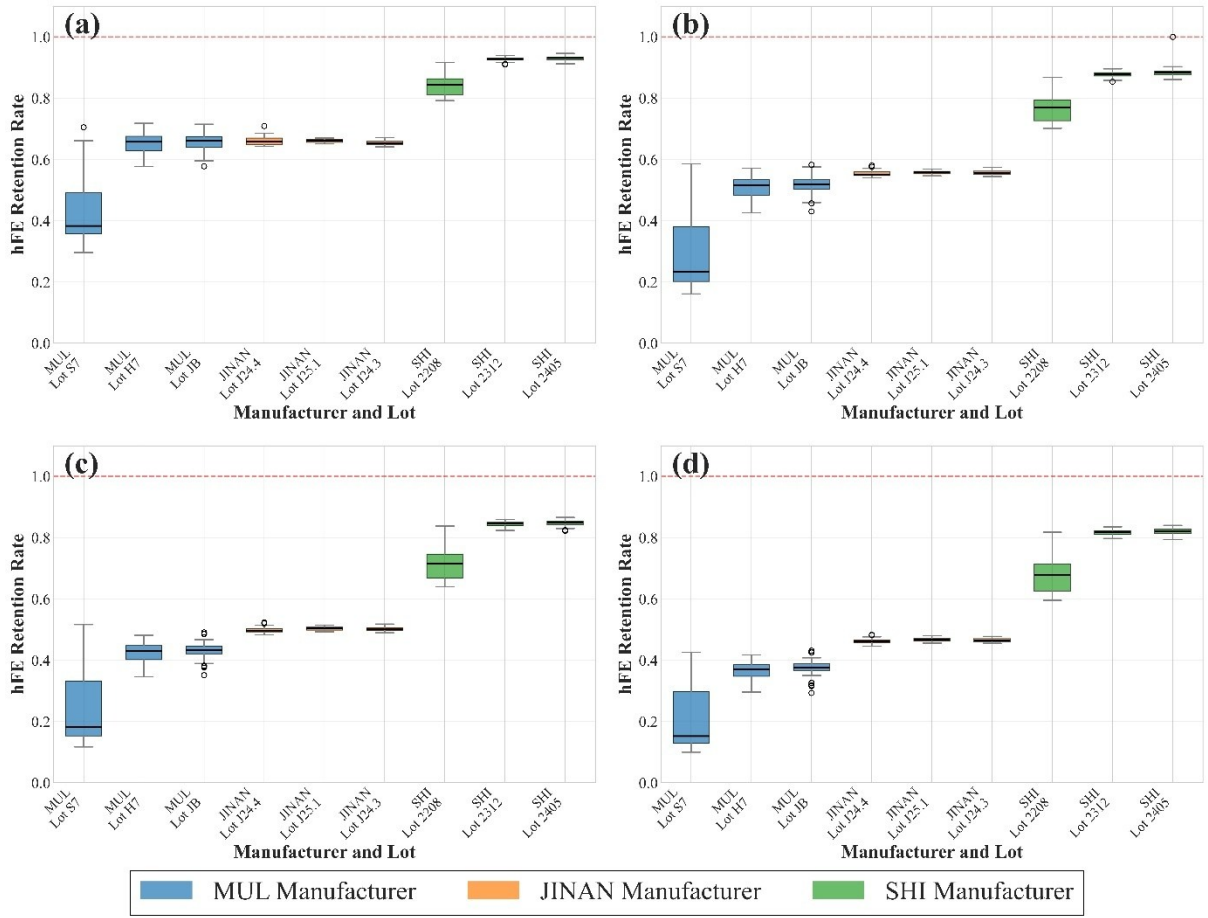


Fig. 14 Distribution of TID radiation degradation patterns across different manufacturers and lots. (a), (b), (c), and (d) show the data distribution of hFE retention rates at 25, 50, 75, and 100 krad, respectively. The median of the boxplot distribution for each lot is represented by a black line, outliers are represented by black hollow circles.

It should be clearly noted that the current model is more suitable for screening and degradation prediction of devices from known lots, and the generalization results for entirely new lots can only serve as a reference for the task. This limitation can be explained by the shifts in electrical parameters and degradation patterns induced by lot-to-lot process variations, as illustrated in Fig. 1, Fig. 2, Fig. 14. The limited generalization ability of the model on lot J24.4 can be attributed to the inclusion in the training and validation sets of lots whose degradation patterns are similar to that of the above lot. In essence, because a purely data-driven model has not been exposed to new lot samples during training, it is difficult for it to learn the specific degradation shift mechanisms of those lots, and consequently it cannot accurately characterize the radiation degradation trends of unknown lots.

IV. Conclusion

This study, by constructing a machine learning model with physical feature enhancement, confirms the potential correlation between the pre-irradiation electrical parameters of COTS BJTs and their RH, and identifies the differences in device radiation hardness induced by manufacturing process variations. The results show that electrical parameter responses under regular electrical stress exhibit significant limitations in characterizing radiation hardness, whereas extracting electrical parameter responses under multiple sets of electrical stresses effectively improves manufacturing process identification capability and TID radiation degradation prediction accuracy. Compared with typical sampling-averaged methods, the model achieves R^2 values higher than 0.8 at

multiple dose points on the test set. The constructed neural network for TID degradation prediction provides a certain cross-lot evaluation reference value, and for new lot devices not covered in the training set, the model exhibits a certain generalization ability, with R^2 values greater than 0 at multiple dose points.

This study represents the first step in the physical feature enhancement approach for TID radiation degradation prediction of COTS devices, focusing on exploring the methodology based on physical feature enhancement and radiation degradation prediction for BJTs. Future research on this topic will pursue the following investigations:

1. Expand the current study dataset by integrating multi-source historical TID radiation experimental data to increase the training sample size, and establish an adaptive calibration mechanism based on lot similarity metrics, thereby improving generalization performance on unknown lots while maintaining within-lot consistency.
2. Enhance dose rate adaptability. In view of the typical low-dose-rate enhancement effect in bipolar devices, multi-dose-rate irradiation experiments will be conducted to construct a degradation dataset covering a wide dose rate range, thereby extending the model's adaptability to different dose rate irradiation conditions.
3. Propose a method migration strategy across device structures. For heterostructure devices such as PNP BJTs and MOSFETs, transfer research will be carried out from three aspects: data acquisition, feature reconstruction, and model fine-tuning, to verify the applicability of the proposed method to a wider range of device types.

References

1. Torrez KV, Ticona Coaquira F, Silva Plata M, et al (2024) Assessing COTS sensor suitability for CubeSat missions in near-space environments. In: 2024 11th International Workshop on Metrology for AeroSpace (MetroAeroSpace). IEEE, Lublin, Poland, pp 490–495
2. Brunetti G, Campiti G, Tagliente M, Ciminelli C (2024) COTS devices for space missions in LEO. IEEE Access 12:76478–76514. <https://doi.org/10.1109/ACCESS.2024.3405373>
3. Bezerra F, Mekki J, Augustin G, et al (2021) Proposal of a lightened radiation hardness assurance methodology for new space. In: 2021 21th European Conference on Radiation and Its Effects on Components and Systems (RADECS). IEEE, Vienna, Austria, pp 1–6
4. Rizzo M, Muschitiello M, Gupta V, Poizat M (2024) A characterization method for TID versus temperature effects on microelectronic circuits. IEEE Trans Nucl Sci 71:1932–1939. <https://doi.org/10.1109/TNS.2024.3418293>
5. Sun B, Moody R, Hiemstra DM, et al (2024) TID response of commercial-of-the-shelf operational amplifiers. In: 2024 IEEE Radiation Effects Data Workshop (REDW) (in conjunction with 2024 NSREC). IEEE, Ottawa, ON, Canada, pp 1–3
6. Barnard A, Steyn WH (2007) Low cost TID testing of COTS components. In: 2007 9th European Conference on Radiation and Its Effects on Components and Systems. IEEE, Deauville, France, pp 1–4
7. Privat A, Barnaby HJ, Adell PC, et al (2019) Multiscale modeling of total ionizing dose effects in commercial-off-the-shelf parts in bipolar technologies. IEEE Trans Nucl Sci 66:190–198. <https://doi.org/10.1109/TNS.2018.2887235>
8. Bokil H (2020) COTS semiconductor components for the new space industry. In: 2020 4th IEEE Electron Devices Technology & Manufacturing Conference (EDTM). IEEE, Penang, Malaysia, pp 1–4
9. Wen Z, Wei D, Liang A, Yewei F (2022) A theoretical framework of COTS components space application based on “risk information entropy.” In: 2022 4th International Conference on System Reliability and Safety Engineering (SRSE). IEEE, Guangzhou, China, pp 353–357
10. Chen Y-L, Sacchi S, Dey B, et al (2024) Exploring machine learning for semiconductor process optimization: A systematic review. IEEE Trans Artif Intell 5:5969–5989. <https://doi.org/10.1109/TAI.2024.3429479>
11. Nakata K, Orihara R, Mizuoka Y, Takagi K (2017) A comprehensive big-data-based monitoring system for yield enhancement in semiconductor manufacturing. IEEE Trans

- Semicond Manuf 30:339–344. <https://doi.org/10.1109/TSM.2017.2753251>
12. Li Z-L, Pei S, Chen Z, et al (2024) Machine learning-assisted amidase-catalytic enantioselectivity prediction and rational design of variants for improving enantioselectivity. *Nat Commun* 15:8778. <https://doi.org/10.1038/s41467-024-53048-0>
 13. Su X, Hu P, Li D, et al (2025) Interpretable identification of cancer genes across biological networks via transformer-powered graph representation learning. *Nat Biomed Eng* 9:371–389. <https://doi.org/10.1038/s41551-024-01312-5>
 14. Fobar D, Vanderlip WJ, Koch W, Chapman P (2022) A machine learning approach to a multidetector array response function for nuclear search. *IEEE Trans Nucl Sci* 69:1939–1944. <https://doi.org/10.1109/TNS.2022.3186831>
 15. Churchill RM, Chang CS, Ku S (2020) Finding structure in large data sets of particle distribution functions using unsupervised machine learning. *IEEE Trans Plasma Sci* 1–4. <https://doi.org/10.1109/TPS.2020.2985625>
 16. Hansen DL, Czajkowski D, Vermeire B (2022) Using machine learning to determine proton cross-sections from heavy-ion data. *IEEE Trans Nucl Sci* 69:264–272. <https://doi.org/10.1109/TNS.2022.3140725>
 17. Yimwadsana B (2023) Leveraging machine learning for estimating relationship model through empirical scientific data. In: 2023 27th International Computer Science and Engineering Conference (ICSEC). IEEE, Samui Island, Thailand, pp 358–361
 18. Leemann SC, Liu S, Hexemer A, et al (2019) Demonstration of machine learning-based model-independent stabilization of source properties in synchrotron light sources. *Phys Rev Lett* 123:194801. <https://doi.org/10.1103/PhysRevLett.123.194801>
 19. Li L, Chen X-C, Yang G-X (2023) Deep-learning model for buildup of ionization defects in bipolar junction transistors. *IEEE Trans Nucl Sci* 70:2175–2182. <https://doi.org/10.1109/TNS.2023.3298707>
 20. Martin-Holgado P, Romero-Maestre A, de-Martin-Hernandez J, et al (2022) How the analysis of archival data could provide helpful information about TID degradation. Case study: Bipolar transistors. *IEEE Trans Nucl Sci* 69:1691–1699. <https://doi.org/10.1109/TNS.2022.3185940>
 21. Morilla F, Vega J, Dormido-Canto S, et al (2024) A machine learning approach to predict radiation effects in microelectronic components. *Sens* 24:4276. <https://doi.org/10.3390/s24134276>
 22. Wang B-C, Qiu M-T, Chen W, et al (2022) Machine learning-based analyses for total ionizing dose effects in bipolar junction transistors. *Nucl Sci Tech* 33:131. <https://doi.org/10.1007/s41365-022-01107-w>
 23. Li X, Yang J, Fleetwood DM, et al (2018) Hydrogen soaking, displacement damage effects, and charge yield in gated lateral bipolar junction transistors. *IEEE Trans Nucl Sci* 65:1271–1276. <https://doi.org/10.1109/TNS.2018.2837032>
 24. Yu X, Li X, Xun M, et al (2025) Energy and dose rate response of photons' total dose radiation effect in bipolar transistors. *Radiat Eff Defects Solids* 180:1560–1572. <https://doi.org/10.1080/10420150.2025.2481082>
 25. Li X, Lu W, Wang X, et al (2017) Using temperature-switching approach to evaluate the ELDRS of bipolar devices. *Radiat Eff Defects Solids* 172:824–834. <https://doi.org/10.1080/10420150.2017.1411354>
 26. Li L, Chen X-C, Jian Y, et al (2021) Modeling the ionization damage on excess base current in p-n-p BJTs for circuit-level simulation. *IEEE Trans Nucl Sci* 68:2220–2231. <https://doi.org/10.1109/TNS.2021.3094402>
 27. Petrov AS, Ulimov VN (2012) Some features of degradation in bipolar transistors at different test conditions for total ionizing dose effect. *Microelectron Reliab* 52:2435–2437. <https://doi.org/10.1016/j.microrel.2012.06.080>
 28. Whittier RJ, Tremere DA (1967) Current gain (hFE) and cutoff frequency (fT) falloff at high current densities. In: 1967 International Electron Devices Meeting. IRE, pp 100–102
 29. Hueting RJE, vanderToorn R (2005) Analysis of the kirk effect in silicon-based bipolar transistors with a nonuniform collector profile. *IEEE Trans Electron Devices* 52:2489–2495.

<https://doi.org/10.1109/TED.2005.857176>

30. Barnaby HJ, Vermeire B, Campola MJ (2015) Improved model for increased surface recombination current in irradiated bipolar junction transistors. *IEEE Trans Nucl Sci* 62:1658–1664. <https://doi.org/10.1109/TNS.2015.2452229>
31. Tolleson BS, Adell PC, Rax B, et al (2018) Improved model for excess base current in irradiated lateral p-n-p bipolar junction transistors. *IEEE Trans Nucl Sci* 65:1488–1495. <https://doi.org/10.1109/TNS.2018.2829110>
32. Wang C, Chen W, Jin X, et al (2017) Dependence on base width and doping concentration of current degradation in gate-controlled lateral PNP bipolar transistors exposed to reactor neutrons and gamma rays. *Energy Procedia* 127:110–119. <https://doi.org/10.1016/j.egypro.2017.08.119>
33. (2008) Exploratory data analysis. In: *The Concise Encyclopedia of Statistics*. Springer New York, New York, NY, pp 192–194
34. Goodfellow I, Bengio Y, Courville A (2016) *Deep learning*. MIT Press
35. Ba JL, Kiros JR, Hinton GE (2016) Layer normalization. undefined. <https://doi.org/10.48550/ARXIV.1607.06450>
36. Srivastava N, Hinton GE, Krizhevsky A, et al (2022) Dropout: A simple way to prevent neural networks from overfitting. *Journal of machine learning research*
37. Kingma DP, Ba J (2017) Adam: A method for stochastic optimization
38. Na GS (2022) Efficient learning rate adaptation based on hierarchical optimization approach. *Neural Networks* 150:326–335. <https://doi.org/10.1016/j.neunet.2022.02.014>